A Visual Analytics Platform for Tracking Orthopedic Implant Kinematics on High-Speed X-Ray During a Simulated Sideways Fall

J. Levine[1,2,3], E. Bliven[1,2,3], A. Fung[5], I. Fleps[6], B. Helgason[5], P. Guy[1,4], P. A. Cripton[1,2,3]
[1]Orthopaedics and Injury Biomechanics Group, [2]School of Biomedical Engineering, [3]Department of Mechanical Engineering and [4]Department of Orthopaedics, University of British Columbia, Vancouver, British Columbia, Canada, [5]Institute of Biomechanics, ETH Zurich, Zurich, Switzerland, [6]Department of Mechanical Engineering, Boston University, Boston Massachusetts

ABSTRACT

Hip fracture is a debilitating injury with a high rate of morbidity, mortality, and chronic illness. Most hip fractures in the elderly occur through an impact to the greater trochanter of the femur due to a sideways fall from a standing position. As orthopedic implants are becoming increasingly common, the biomechanical properties at the interface between the bone and implant during traumatic injury are relatively unknown. This study investigated the kinematics of an orthopedic implant during a simulated sideways fall impact using high-speed x-ray video analysis. An inertial-based testing apparatus developed during a previous study was used to simulate a sideways fall impact from standing height. Cadaveric specimens were instrumented on the impacting side with an intramedullary fracture fixation implant. A custom bilateral high-speed x-ray system was used to capture impact phenomena from each trial. After each experiment, undistorted x-ray videos were segmented into an array of frames and uploaded to a custom visual analytics platform developed in MATLAB for this study. Here, the implant-bone kinematics were tracked throughout the duration of the fall and impact. Using known dimensions of the implant, the visual analytics tool outputs the translation and rotation of the implant within the frame in two-dimensions. Understanding the kinematics at the bone-implant interface may inform the design of future orthopedic implants to mitigate the potential for periprosthetic fracture.

INTRODUCTION

Hip fracture is a debilitating injury with a high rate of morbidity, mortality, and chronic illness. Previous studies have found that the mortality rate associated with this injury is 12 to 36% within one year of hip fracture (Richmond et al., 2003). In addition, those that do survive, live with decreased mobility, often relying on others for their primary care. It is estimated that by 2041, over 88,000 Canadians will fracture their hip annually, leading to an economic burden of over $2.4 billion (Klotzbuecher et al., 2010).

Most instances of hip fracture can be correlated to a variety of factors including inactivity (Lyritis et al., 1996), cortical bone thickness (Bell et al., 1999), soft tissue thickness over the greater trochanter (Bouxsein et al., 2007), and previous fracture of the contralateral hip (Sobolev et al., 2015). The most influential risk factor that this project aims to mitigate is the instance of

secondary hip fracture after initial fracture on the contralateral side. Studies have found that close to 34% of individuals will suffer an additional fracture in the contralateral hip within 10 years of hip fracture (Sobolev et al., 2015). The majority of hip fractures occur on the greater trochanter of the femur and are instigated by sideways fall from a standing position (Parkkari et al., 1999). The ability to accurately predict and prevent these fractures is necessary to maintain the health of Canada's aging population.

For patients deemed to be of high risk for hip fracture, a variety of prophylactic approaches have been proposed for its prevention. One such method is Femoroplasty, the cement-augmentation of the proximal femur (Heini et al., 2004). While this method has shown to be beneficial in increasing peak fracture loads, it can introduce trochanteric fractures as well as risks from increased temperatures (Szpalski et al., 2015). More rudimentary methods include the introduction of hip pads or protectors, a concept based on dampening impact forces (Cianferotti et al., 2015). However, the efficacy of this approach relies on user compliance (Haines et al., 2006). A more recent method that will be explored by this project, is the use of an orthopedic implant to prevent contralateral hip fracture. A previous study by Szpalski et al. (2015) explored using the Y-STRUT® (Hyprevention®, Pessac, France) orthopedic implant as a hip fracture prophylactic approach. Implant position within the femoral neck was determined using finite element analysis (FEA) and tested using a single stance loading apparatus. Their results indicated that the introduction of a prophylactic implant could increase the load and energy required for fracture to occur.

With the rise of hip fracture cases in Canada, orthopedic implants are becoming an increasingly common therapeutic intervention (Klotzbuecher et al., 2010). A barrier in orthopedic implant design is that the biomechanical properties at the interface between the bone and implant, specifically during injurious events such as hip fracture, are relatively unknown (Gao et al., 2019). Devastating injuries such as periprosthetic fractures, a fracture that occurs in association with a prosthetic implant, can be considered a result of the lack of information surrounding bone-implant interfaces (Della Rocc et al., 2011). These fractures are associated with high morbidity and mortality, with long term mortality rates nearing those of hip fracture (Griffiths et al., 2013). Studies such as one by Bojan et al (2018) investigated the long-term translation of the Stryker Gamma3 Nail within the bone through a year-long x-ray study on a group of 20 patients. The study began by taking the first static x-ray 24 hours post-implantation then proceeded to take static x-rays on 4 additional occasions during the year. In contrast to the static nature of Bojan's study, the current project focused on describing the dynamic kinematics of the implant during a high-speed loading scenario.

In this study a visual analytics platform was developed to document the kinematics of an intramedullary orthopedic nailing system during a simulated sideways fall impact using biplanar high-speed x-ray video analysis. The nailing system was implanted into an intact femur as a model of a prophylactic approach. By comparing the motion of the orthopedic implant to fracture propagation, the implant motion could be described quantitatively during a common injury scenario. Understanding the kinematics at the bone-implant interface may inform the design of future orthopedic implants. This could have the potential to reduce the likelihood of periprosthetic fracture by both understanding the instances of periprosthetic fracture and by increasing the implant's ability to protect the bone during a common injury scenario.

METHODS

The methodology of this project primarily revolved around tracking relative motion at the bone-implant interface using high-speed x-ray video files captured using a custom biplanar x-ray system (Whyte, et al., 2019). To do this, 5 cadaveric specimens were tested using an inertial-based sideways fall simulator that was designed in a previous study (Fleps et al., 2018, 2019). Each specimen was instrumented on the impacting side with an orthopedic implant and encapsulated in a soft tissue surrogate made of ballistic gel. Metal beads were glued to the bone within the soft tissue surrogate. Load at the impact surface was recorded at 10,000 Hz using a force plate. The impact was captured using two bilateral x-rays (labeled 8243 and 8244) at a rate of 8,500 frames per second (fps). The force plate and x-rays were chronologically matched using a trigger that was activated during the descent phase of the fall. The data collection and analysis steps involved in this project include: 1. Video segmentation and undistortion, 2. MATLAB GUI development and use, and 3. Error evaluation and approximation.

Video Segmentation and Undistortion

Video Segmentation was performed in Phantom Camera Control (PCC) software (Version 3.6, AMETEK Material Analysis Division, Wayne, New Jersey) using the following steps. First, high-speed x-ray cine files were imported into the PCC software and spliced so that the first frame exported was at time zero (initiation of the trigger). Next, based on the length of the video, a .jpg image was exported either every 200 or every 150 frames. Finally, while scanning through each video, the start and stop frames of impact were noted. These values were used in determining the timescale in the MATLAB GUI (MathWorks Inc, Natick, Massachusetts, Version R2021b) which will be described in a later section.

Undistortion was performed in XMALab (Knörlein et al., 2016) using the following steps. First, x-ray stills were taken with a metal mesh grid prior to initiation of the experiment and after alignment of each x-ray source-image intensifier pair. Next, these images were uploaded into XMALab and specified as to which camera they are for. Finally, the software took an input of an image folder for a specified camera and undistorts all images in that folder, exporting them as ".tif" files.

MATLAB GUI Development and Use

A MATLAB GUI was developed specifically for this project using built-in app developer software. This program was created to track and analyze user-defined points on the implant and bone. It used the file of undistorted image files exported from XMALab and outputted both a .csv file and a graph of the data collected. In the opening page of this program, the user defined the folder containing the image files they wanted to examine. The user then inputted the specimen's name, camera number, start frame, stop frame, recording frequency, and number of frames that was used.

Next, the user would click *"Add Title"* and move on to the *"Choose Points"* tab (Figure 1). Here, the user would first choose the screw diameter button and specify the diameter of the lag screw of the orthopedic implant (Figure 2). This was used to calculate the actual distances based on the relationship between the known diameter of the screw, 10.5 mm, and the diameter specified by its pixel value in the image. By dividing the pixel value by the actual value, a scale was created and used to calculate the actual distances. Next, the user defined the angle between the implant using three points, one on the trochanteric nail of the implant, one at the intersection between the nail and the lag screw, and on the lag screw. Because there is tapering in both the nail and screw, it was important that these points were chosen in the flat areas close to the intersection. Following this, the user would then click either the *"Bead: 1 Point"* or the *"Bead: 2 Points"* button. If the *"Bead: 1 Point"* button was chosen, the distance between the intersection between the lag screw and trochanteric nail and a chosen bead is calculated. If the *"Bead: 2 Points"* button was chosen, the user defined both points used to calculate the distance. This method was expected to have more error as an arbitrary point on the implant would be used.

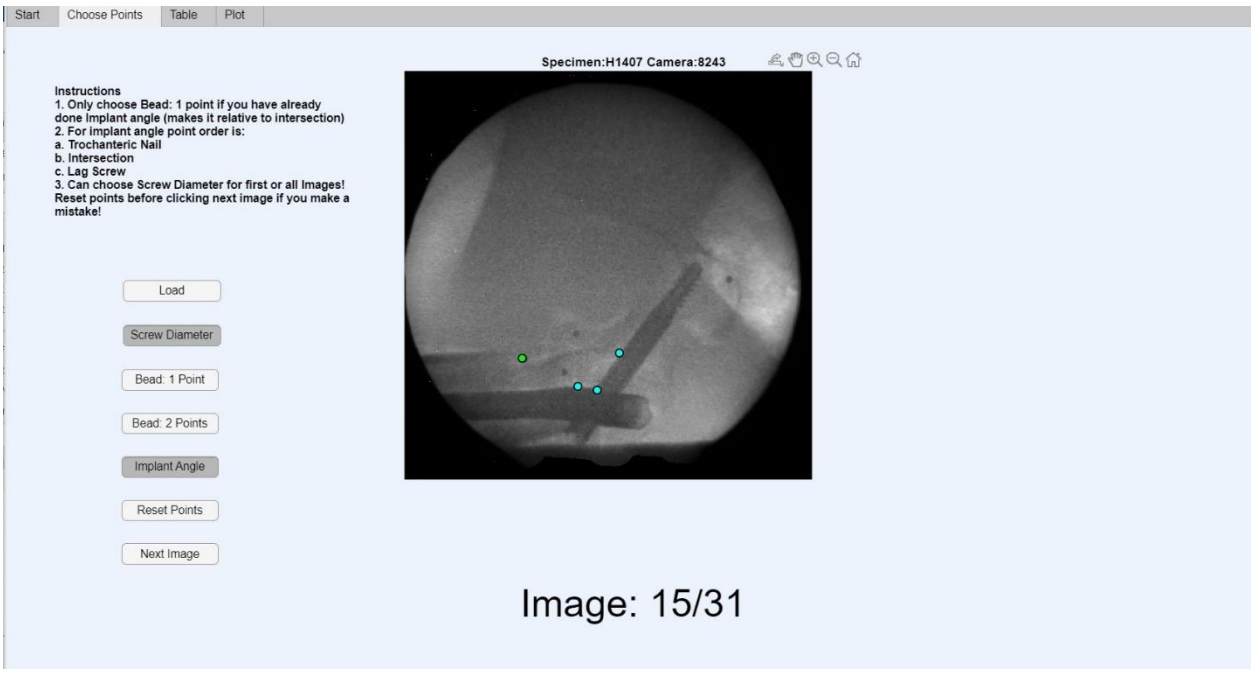

Figure 1: MATLAB GUI Choose Points tab. Cyan markers indicate implant angle. Green Marker indicates location of a metal bead.

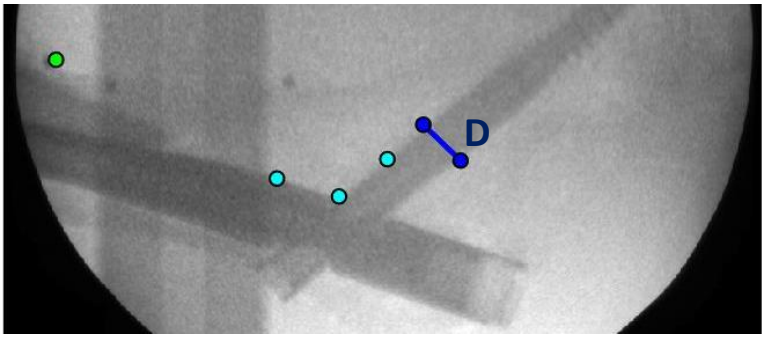

Figure 2: Diameter of the lag screw on the implant, indicated by the letter D on the image above.

Once all points were defined, the user would click the *"Next Image"* button and all the data from the current frame was saved to a table on the following tab. It should be noted that for the implant angle, the order of the points chosen matters. Next, the angle between the implants was calculated as follows where x_1, and y_1 indicated the first point, x_2 and y_2 indicated the second point and x_3 and y_3 indicated the third point:

$$slope\ 1 = \frac{y_2 - y_1}{x_2 - x_1}$$

$$slope\ 2 = \frac{y_3 - y_2}{x_3 - x_2}$$

$$\theta = 180 + \tan^{-1}\left(\frac{slope\ 2 - slope\ 1}{1 + slope\ 2 \times slope\ 1}\right) \times \frac{180}{\pi}$$

All data calculated and retrieved from this program were exported as a .csv file through the *"Table"* tab. The user was then able to view the change in implant angle and change in bead distance over time in the *"Plot"* tab. In data analysis, a lowpass filter was applied to the angle-time data in MATLAB with a cut-off value of 0.25 to the angle data.

Error Evaluation

This software required user-defined points for its calculations leading to a potential of human error. To account for and analyze this error, a population of n = 5 users was chosen to run the code. The specifications of the frames chosen were every 200 frames for a total of 30 frames to review. For the first frame, the user specified the screw diameter and the implant angle using the *"Screw Diameter"* and *"Implant Angle"* buttons. For each consecutive frame, the user specified the implant angle and the location of the metal bead attached to the bone using the *"Bead: 1 Point"* button. Maximum and minimum values, as well as standard deviation was calculated for the angle, the normalized angle, and the bead distance (mm) for each user's trial.

To evaluate the efficacy of the scaling factor, the *"Bead: 2 Points"* button was used and the two end points of the lag screw were selected. That output distance value was then compared to the actual length of the nail. Additionally, the calculated angle was compared to the implanted

angle between the trochanteric nail and lag screw, which was known to be 125 degrees for all specimens.

To evaluate precision, one of the users that was previously chosen, repeated the same trial done previously a total of 5 times. Three times where every 100th frame is chosen, and twice where every 200th frame is chosen.

RESULTS

Variation Between Specimens

The following table (Table 1) and figure (Figure 3) summarize the main values used to compare the results from tests between specimens. The figure shows the angle variation after the application of a lowpass filter. The data from the table is prior to application of the lowpass filter.

Table 1: Data variation between specimens.

Specimen	Scale	Min Angle	Max Angle	Angle Standard Deviation	Fracture Status
1	3.86	116.57	128.36	2.74	No
2	3.43	114.71	129.14	3.17	Yes
3	4.43	116.89	128.76	3.24	Yes
4	5.06	114.11	127.27	3.47	No
5	4.86	114.73	132.15	4.03	No

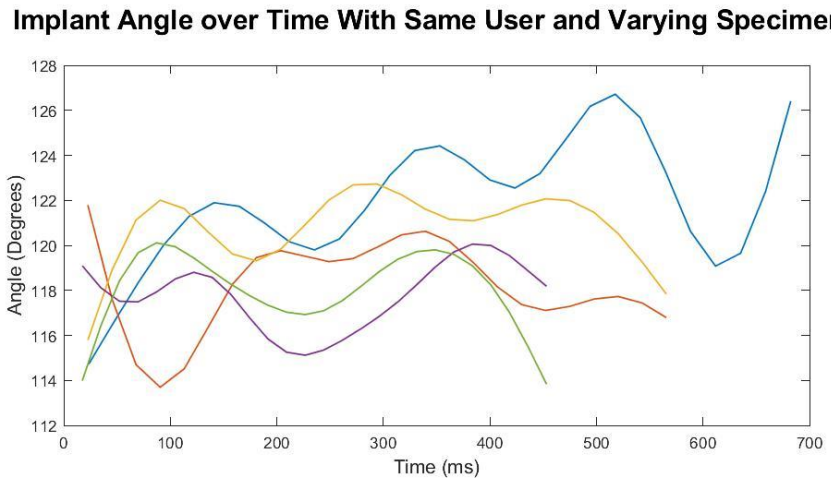

Figure 3: Implant angle over time – comparison between specimens.

Inter-User Variation

The following table (Table 2) and figure (Figure 4) summarize the main values used to compare the results from having multiple different users' test the code. All tests were performed using specimen 5 and camera 8244. The figure shows the angle variation after the application of a lowpass filter. The data from the table is prior to application of the lowpass filter.

Table 2: Inter-user data variation.

User Number	Scale	Min Angle	Max Angle	Angle Standard Deviation
1	5.47	114.72	132.15	4.03
2	4.91	120.65	131.11	2.47
3	5.60	109.57	130.69	3.98
4	4.72	104.01	146.72	7.41
5	4.43	119.97	132.33	3.08

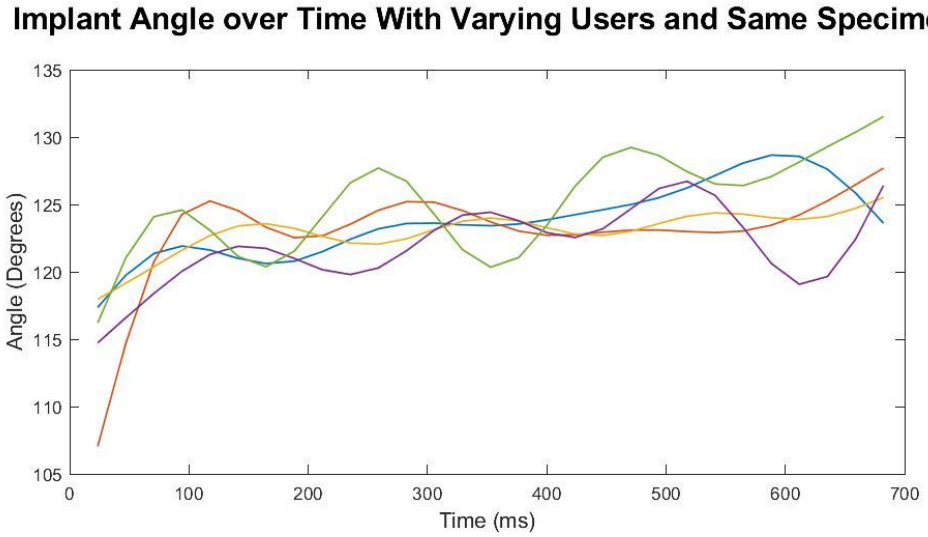

Figure 4: Implant angle over time – comparison between users.

Intra-User Variation

The following table (Table 3) and figure (Figure 5) summarize the main values used to compare the results from having the same user test the code multiple times. All tests were performed using specimen 5 and camera 8244 where there were variations in the number of frames used. The figure shows the angle variation after the application of a lowpass filter. The translucent lines represent the area containing all values from each number of frames chosen.

The opaque lines represent the average value from each number of frames chosen. The data from the table is prior to application of the lowpass filter.

Table 3: Intra-user data variation.

Trial Number	Number of Frames Used	Scale	Min Angle	Max Angle	Angle Standard Deviation
1	30	5.47	114.7	132.2	4.1
2	30	4.32	113.7	132.2	3.6
3	62	5.10	116.4	131.6	3.2
4	62	5.69	116.4	132.8	3.2
5	62	4.41	112.2	129.6	3.1

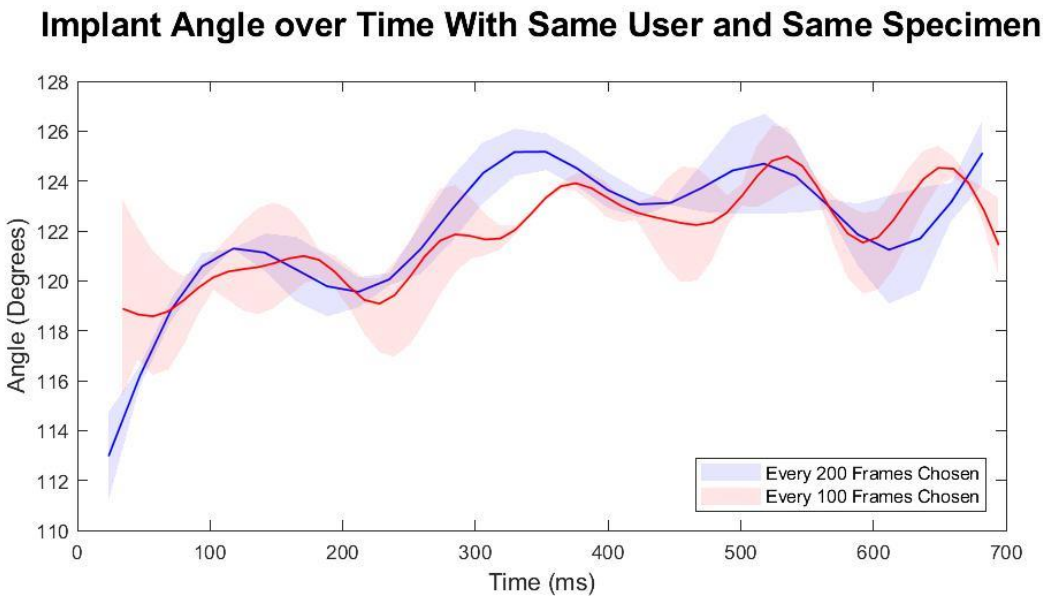

Figure 5: Implant angle over time – variation within same user.

Scaling Results

The following table summarizes the results from testing the use of the diameter of the lag screw as a scaling factor. All implants used for this study had an angle of 125 degrees between the trochanteric nail and lag screw listed in the product specification on their packaging.

Table 4: Scale experimentation results.

Specimen	Scale	Angle (Prior to impact)	Screw Length (Pixels)	Screw Length (mm)	Actual Screw Length (mm)
1	4.53	118	417.8	92.2	80
2	4.81	113.8	414.0	86.07	85
3	4.711	122.3	413.6	87.8	100
4	5.31	123.10	474.2	89.3	95
5	4.83	125.68	489.8	101.8	100

DISCUSSION

The aim of this study was to develop a visual analytics platform to investigate the bone-implant kinematics of an intramedullary orthopedic nailing system during a simulated high-speed injurious event. Through development of the MATLAB GUI, data analysis, and filtering of the results, we were able to describe the motion of the implant during impact. Validation tests allowed us to describe the repeatability and precision differences in the intra- and inter-user trials. Comparing the trials between the specimens allowed for a preliminary determination on the relationship between implant motion and fracture outcome.

From the variation between specimens, it could be seen that the angle deviation through the fall and impact followed a wave-like pattern. While this did not correlate with fracture status, the number and amplitude of the peaks could be chronologically matched to the force plate data to determine if a change in the impact force influenced the implant angle. For the intra- and inter-user validation trials, when selecting the screw-nail angle, intra-user angle deviations were generally lower than values between different users, suggesting that the program can be used consistently. Additionally, from the intra-user validation trial, when a higher number of frames were selected (every 100 frames), more variations in the angle curve were seen and lower standard deviations were reported. From this, it can be inferred that as the number of frames increased, a more descriptive view of the motion was produced.

In contrast to previous studies (Bojan et al., 2018) which were able to quantitatively describe the long-term motion of the implant within the bone using a series of static x-rays, our program has the potential to describe similar motion parameters in a dynamic, impact scenario. The exact values of these parameters will require more validation experiments in the future, as this study was limited by its description using only one of the two biplanar x-rays. The x-ray used for the results section of this study was almost directly perpendicular to the plane of motion of the specimen during its fall. Because of this, it was assumed that the angles calculated from this x-ray are most similar to the actual values. Regarding this, there were limitations in that the specimen was only rotationally constrained during the preimpact motion and was released from the guild plane just prior to impact. This means that once the specimen left the guide rail and impacted the force plate, it was able to rotate freely, leading to a higher likelihood of it being out of alignment with its initial plane of movement. This rotation may have distorted the calculated angle within the two-dimensional view. This could be examined further in future studies by comparing the angle in three-dimensions to the angles calculated in this study.

Like the study by Whyte et al (2019), the implantation of metal beads in the cadaveric tissue was necessary to identify key points to track within the x-ray during a high-speed impact. For tracking key points on the implant, the main location that was always visible, which was used as a reference, was the intersection of the trochanteric nail and lag screw. A limitation with this was that the distance between this intersection and any of the metal beads provided less accurate data than if a key point had been used at the distal end of the trochanteric nail. This is because some of the x-ray videos suggested a toggling motion of the distal tip of the implant

within the medullary cavity. To track this point, the other camera (not perpendicular to motion) would have had to be used. As the x-ray protocol was still in development during these trials, there was a lower contrast in this camera which led to difficulties in identifying key features.

Regarding human error, the similarities between the inter- and intra-user trials shows promise in the repeatability of this approach. While the use of user-selected points was a limitation in this current study, there are a variety of approaches that can be used to mitigate the potential errors associated with this. These could be the addition of a "zoom-in" function and thresholding parameters to let the user know when the calculated angle is out of a given range.

CONCLUSIONS

The framework developed in this project was able to obtain replicable values that describe relative bone-implant motion in two dimensions. Future work will focus on error reduction, statistical analysis, ground truth validation, three-dimensional projections, and correlation with force plate data. Based on the results from this study and the potential for future improvements, this model was effective in its ability to describe the locations of key points on the implant and the bone during motion. Using this program has the potential to reduce the likelihood of periprosthetic fracture by increasing our understanding of bone-implant kinematics during a common injury scenario.

ACKNOWLEDGEMENTS

The authors would like to thank Dr. Robyn Newell for her expertise and assistance throughout all aspects of this study. The sideways fall experiments were partially funded by Funding from the Swiss National Science Foundation (grant nr. 205320_169331).

REFERENCES

BELL, K. L., LOVERIDGE, N., POWER, J., GARRAHAN, N., STANTON, M., LUNT, M., . . . REEVE, J. (1999). Structure of the Femoral Neck in Hip Fracture: Cortical Bone Loss in the Inferoanterior to Superoposterior Axis. *Journal of Bone and Mineral Research*, 111-119.

BOJAN, A. J., JÖNSSON, A., GRANHED, H., EKHOLM, C., & KÄRRHOLM, J. (2018). Trochanteric fracture-implant motion during healing – A radiostereometry (RSA) study. *Injury*, 673-679.

BOUXSEIN, M. L., SZULE, P., MUNOZ, F., THRALL, E., SORNAY-RENDU, E., & DELMAS, P. D. (2007). Contribution of Trochanteric Soft Tissues to Fall Force Estimates, the Factor of Risk, and Prediction of Hip Fracture Risk. *Journal of Bone and Mineral Research*, 825-831.

CIANFEROTTI, L., FOSSI, C., & BRANDI, M. L. (2015). Hip Protectors: Are They Worth it? *Calcified tissue international*, 1-11.

DELLA ROCC, G. J., LEUNG, K. S., & PAPE, H.-C. (2011). Periproshteic Fractures: Epidemiology and Future Projections. *Journal of ORthopaedic Trauma*, S66-S70.

FLEPS, I., GUY, P., FERGUSON, S. J., CRIPTON, P. A., & HELGASON, B. (2019). Explict Finite Element Models Accurately Predict Subject-Specific and Velocity-Dependent Kinetics of Sideways Fall Impact. *Journal of Bone and Mineral Research*, 1837-1850.

FLEPS, I., VUILLE, M., MELNYK, A., FERGUSON, S. J., GUY, P., HELGASON, B., . . . PÉREZ, M. A. (2018). A novel sideways fall simulator to study hip fractures ex vivo. *PLOS ONE*, e0201096.

GAO, X., FRAULOB, M., & HAÏAT, G. (2019). Biomechanical behaviours of the bone–implant interface: a review. *Journal of The Royal Society Interface*, 20190259.

GRIFFITHS, E. J., CASH, D., KALRA, S., & HOPGOOD, P. J. (2013). Time to surgery and 30-day morbidity and mortality of periprosthetic hip fractures. *Injury*, 1949-1952.

HAINES, T. P., HILL, K. D., BENNELL, K. L., & OSBORNE, R. H. (2006). Hip protector use amongst older hospital inpatients: compliance and functional consequences. *Age and Ageing*, 520-523.

HEINI, P. F., FRANZ, T., FANKHAUSER, C., GASSER, B., & GANZ, R. (2004). Femoroplasty-augmentation of mechanical properties in the osteoporotic proximal femur: A biomechanical investigation of PMMA reinforcement in cadaver bones. *Clinical Biomechanics*, 506-512.

HUISKES, R. (1986). Biomechanics of Bone-Implant Interactions. *Frontiers in Biomehcanics*, 245-262.

KLOTZBUECHER, C. M., ROSS, P. D., LANDSMAN, P. B., ABBOTT, T. A., & BERGER, M. (2010). Patients with Prior Fractures Have an Increased Risk of Future Fractures: A Summary of the Literature and Statistical Synthesis. *Journal of Bone and Mineral Research*, 721-739.

KNÖRLEIN, B. J., BAIER, D. B., GATESY, S. M., CHASEN, J. L., & BRAINERD, E. L. (2016). Validation of XMALab software for marker-based XROMM. *J Exp Biol* , 3701–3711.

LYRITIS , G P; MEDOS STUDY GROUP. (1996). Epidemiology of hip fracture: The MEDOS study. *Osteoporosis International*, 11-15.

PARKKARI, J., KANNUS, P., PALVANEN, M., NATRI, A., VAINIO, J., AHO, H., . . . JÄRVINEN, M. (1999). Majority of Hip Fractures Occur as a Result of a Fall and Impact on the Greater Trochanter of the Femur: A Prospective Controlled Hip Fracture Study with 206 Consecutive Patients. *Calcified Tissue International*, 183-187.

PARKKARI, J., KANNUS, P., PALVANEN, M., NATRI, A., VAINIO, J., AHO, H., . . . JÄRVINEN, M. (1999, 09). Majority of Hip Fractures Occur as a Result of a Fall and Impact on the Greater Trochanter of the Femur: A Prospective Controlled Hip Fracture Study with 206 Consecutive Patients. *Calcified Tissue International, 65*(3), 183-187. doi:10.1007/s002239900679

RICHMOND, J., AHARONOFF, G., ZUCKERMAN , J., & KOVAL, K. (2003). Mortality Risk After Hip Fracture. *Journal of Orthopaedic Trauma*, S2-S5.

SOBOLEV, B., SHEEHAN, K. J., KURAMOTO, L., & GUY , P. (2015). Risk of second hip fracture persists for years after initial trauma. *Bone*, 72-76.

SZPALSKI, M., GUNZBURG, R., AEBI, M., DELIMOGE, C., GRAF, N., EBERLE, S., & VIENNEY, C. (2015). A new approach to prevent contralateral hip fracture: Evaluation of the effectiveness of a fracture preventing implant. *Clinical Biomechanics*, 713-719.

WHYTE, T., LIU, J., CHUNG, V., MCERLANE, S. A., ABEBE, Z. A., MCINNES, K. A., . . . CRIPTON, P. A. (2019). Technique and preliminary findings for in vivo quantification of brain motion during injurious head impacts. *Journal of Biomechanics*, 109279.